

# A V-Band Front-End With 3-D Integrated Cavity Filters/Duplexers and Antenna in LTCC Technologies

Jong-Hoon Lee, *Student Member, IEEE*, Nobutaka Kidera, Gerald DeJean, *Student Member, IEEE*, Stéphane Pinel, *Member, IEEE*, Joy Laskar, *Fellow, IEEE*, and Manos M. Tentzeris, *Senior Member, IEEE*

**Abstract**—This paper presents a compact system-on-package-based front-end solution for 60-GHz-band wireless communication/sensor applications that consists of fully integrated three-dimensional (3-D) cavity filters/duplexers and antenna. The presented concept is applied to the design, fabrication, and testing of V-band (receiver (Rx): 59–61.5 GHz, transmitter (Tx): 61.5–64 GHz) transceiver front-end module using multilayer low-temperature co-fired ceramic technology. Vertically stacked 3-D low-loss cavity bandpass filters are developed for Rx and Tx channels to realize a fully integrated compact duplexer. Each filter exhibits excellent performance (Rx: IL < 2.37 dB, 3-dB bandwidth (BW)  $\sim$  3.5%, Tx: IL < 2.39 dB, 3-dB BW  $\sim$  3.33%). The fabrication tolerances contributing to the resonant frequency experimental downshift were investigated and taken into account in the simulations of the rest devices. The developed cavity filters are utilized to realize the compact duplexers by using microstrip T-junctions. This integrated duplexer shows Rx/Tx BW of 4.20% and 2.66% and insertion loss of 2.22 and 2.48 dB, respectively. The different experimental results of the duplexer compared to the individual filters above are attributed to the fabrication tolerance, especially on microstrip T-junctions. The measured channel-to-channel isolation is better than 35.2 dB across the Rx band (56–58.4 GHz) and better than 38.4 dB across the Tx band (59.3–60.9 GHz). The reported fully integrated Rx and Tx filters and the dual-polarized cross-shaped patch antenna functions demonstrate a novel 3-D deployment of embedded components equipped with an air cavity on the top. The excellent overall performance of the full integrated module is verified through the 10-dB BW of 2.4 GHz ( $\sim$  4.18%) at 57.45 and 2.3 GHz ( $\sim$  3.84%) at 59.85 GHz and the measured isolation better than 49 dB across the Rx band and better than 51.9 dB across the Tx band.

**Index Terms**—Bandpass filter (BPF), cavity filters, dual-band antenna, duplexer, front-end module, integrated passives, low-temperature co-fired ceramic (LTCC), millimeter wave, patch antenna, system-on-package (SOP), three-dimensional (3-D) integration, transceiver, V-band.

## I. INTRODUCTION

LATELY THERE has been a growing interest for broadband and high-data rate ( $>2$  Gb/s) wireless services such as a high-speed Internet, real-time video streaming, high-definition television (HDTV), wireless gigabit Ethernet, and automotive

sensor [1]–[3]. The unlicensed spectrum around 60 GHz is very well suited for such applications, especially for short ranges, because of its wider bandwidth than other wireless local area network (WLAN)/wireless personal area network (WPAN) standards [1]. In the 60-GHz band, wireless communication systems call upon miniaturization, portability, cost-saving, and performance improvement to satisfy the specifications of the next-generation multigigabit per second wireless transmission [4]. The three-dimensional (3-D) integration approach using multilayer low-temperature co-fired ceramic (LTCC) technologies has emerged as an attractive solution for these systems due to its high level of compactness and mature multilayer fabrication capability. However, the optimal integration of RF passives including duplexers and antennas into a 3-D 60-GHz (V-band) front-end module is significantly challenging since the electrical performance can be degraded by severe parasitic, interconnection, and radiation losses. The stringent isolation requirement between Rx (59–61.5 GHz) and Tx (61.5–64 GHz) channel signals of 5-GHz-band transceivers also requires the design of a highly integrated duplexer consisting of on-package low-loss and narrowband filters. The duplexer not only serves as a 3-D interconnect between the Rx/Tx monolithic-microwave integrated-circuit (MMIC) chipsets and the antenna, but also as an effective means to minimize the level of the interference between two channels. Fig. 1 shows the simplified block diagram of a V-band front-end system that includes a dual-band antenna, a duplexer, and integrated RF active devices such as a power amplifier (PA), low-noise amplifier (LNA), and mixers. The development of 60-GHz-band modules for stringent system specifications has been demonstrated in a system-in-package (SIP) transmitter integrating LTCC patch arrayed antennas [5] and compact wireless transceiver modules for gigabit data-rate transmission [6]–[8]. However, the previously reported transmitter and receiver modules could suffer from the spurious and image signals because only antennas are integrated into modules without using any band select filters or duplexers in passive front-ends. Moreover, two separate antennas for the Tx and Rx channels are used and occupy a large area, which contradicts the size requirements of compact 60-GHz modules. In addition, a 60-GHz duplexer based on nonradiative dielectric (NRD) guide technology was constructed for a wireless broadband asymmetric digital subscriber line (ADSL) [9]. Recently, personal communications systems (PCS) duplexers based on surface acoustic wave (SAW) [10], [11] and film bulk acoustic resonator (FBAR) [12] filters combined with an LTCC package are reported with excellent Tx-to-Rx isolation for L-band applications. However, the fully integrated 3-D cavity duplexer and dual-polarized antenna functions have not been reported

Manuscript received December 20, 2005. This work was supported by the Asahi Glass Company, by the Georgia Institute of Technology Packaging Research Center, by the Georgia Electronic Design Center, by the National Science Foundation (NSF) under NSF CAREER Award ECS-9984761, and by the NSF under Grant ECS-0313951.

J.-H. Lee, G. DeJean, S. Pinel, J. Laskar, and M. M. Tentzeris are with the Georgia Electronic Design Center, School of Electrical and Computer Engineering, Georgia Institute of Technology, Atlanta, GA 30332 USA (e-mail: jonlee@ece.gatech.edu; pinel@ece.gatech.edu; joy.laskar@ece.gatech.edu).

N. Kidera is with the Asahi Glass Company Ltd., 221-8755 Yokohama, Japan. Digital Object Identifier 10.1109/TMTT.2006.877440

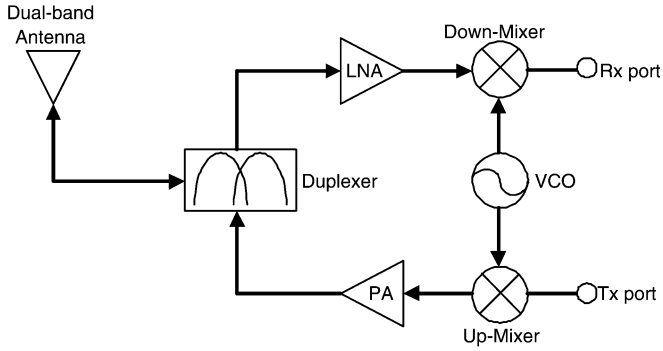


Fig. 1. V-band transceiver block diagram on LTCC multilayer board.

yet as a system-on-package (SOP) compact front-end solution for the LTCC-based V-band modules.

In this paper, we present the complete 3-D integration of all passive building blocks such as the cavity duplexers and the antennas, enabling the complete passive front-end solution for compact 3-D 60-GHz-band transceiver front-end modules. In Section II, a vertically stacked 3-D low-loss cavity bandpass filter (BPF) [13], [14] for Rx and Tx channels is designed and easily integrated into a V-band module as a fundamental component of a duplexer. Section III concentrates on the design of the duplexer consisting of two resonant three-pole cavity filters similar to those developed in Section II and a microstrip T-junction, which connects the two filters and the common input reserved for an antenna. The fully integrated Rx and Tx filters and the dual-polarized antenna are then demonstrated in Section IV with a measured Tx-to-Rx isolation better than 49 dB across the Rx band and better than 51.9 dB across the Tx band.

## II. THREE-POLE CAVITY BPF

The proposed vertically stacked cavity BPF is designed in a way that allows for its easy integration with a V-band multilayer module due to its compactness and its 3-D interconnect feature as a duplexer between the active devices on the top of the LTCC board and the antenna integrated on the back side. A high level of compactness can be achieved by vertically stacking three identical cavity resonators with the microstrip feedlines vertically coupled through rectangular slots etched on the input and output resonators. The proposed devices were fabricated in an LTCC by the Asahi Glass Company, Yokohama, Japan. The relative permittivity ( $\epsilon_r$ ) of the substrate is 5.4 and its loss tangent ( $\tan \delta$ ) is 0.0015. The dielectric layer thickness per layer is  $100 \mu\text{m}$ , and the metal thickness is  $9 \mu\text{m}$ . The resistivity of metal (silver trace) is determined to be  $2.7 \times 10^{-8} \Omega \cdot \text{m}$ . All designs are optimized with the aid of the finite-element method (FEM)-based full-wave High Frequency Structure Simulator (HFSS).

### A. Design of Cavity Resonator

The cavity resonator (see Fig. 2) that is the most fundamental component of the cavity filter is built based on the conventional rectangular cavity resonator approach [15]. The cavity resonator shown in Fig. 2 consists of one LTCC cavity, two microstrip lines for input and output, and two vertically coupling slots etched on the ground planes of the cavity. The resonant

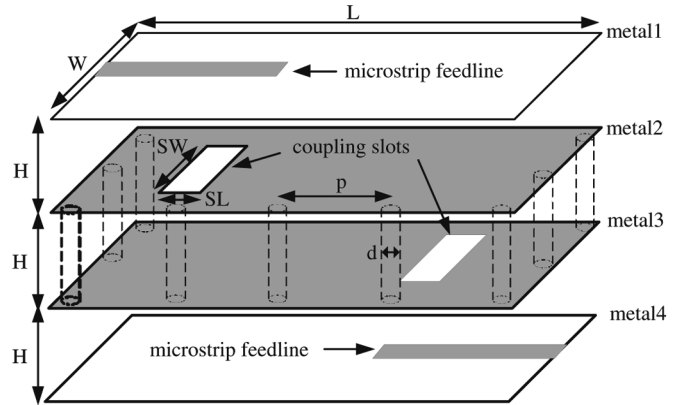


Fig. 2. 3-D overview of LTCC cavity resonator employing slot excitation with microstrip feedlines.

frequency of the fundamental  $\text{TE}_{101}$  mode can be determined by [15]

$$f_{\text{res}} = \frac{c}{2\pi\sqrt{\epsilon_r}} \sqrt{\left(\frac{m\pi}{L}\right)^2 + \left(\frac{n\pi}{H}\right)^2 + \left(\frac{l\pi}{W}\right)^2} \quad (1)$$

where  $f_{\text{res}}$  is the resonant frequency,  $c$  is the speed of light,  $\epsilon_r$  is the dielectric constant,  $L$  is the length of cavity,  $W$  is the width of cavity,  $H$  is the height of cavity, and  $m = l = 1$ ,  $n = 0$  are the indices for the  $\text{TE}_{101}$  mode. The resonant frequency at 60.25 GHz establishes the initial dimensions of the cavity resonator enclosed by perfectly conducting walls. For the purpose of compactness, the height ( $H$ ) is determined to be 0.1 mm (one substrate layer). The vertical conducting walls are then replaced by double rows of via posts that are sufficient to suppress the field leakage and to enhance the quality factor ( $Q$ ) [16]. In addition, the size and spacing of via posts are properly chosen to prevent electromagnetic field leakage and to achieve the stop-band characteristic at the desired resonant frequency according to the guidelines specified in [16]. In our study, the minimum value ( $390 \mu\text{m} = p$  in Fig. 2) of center-to-center vias spacing and the minimum value ( $130 \mu\text{m} = d$  in Fig. 2) of the via diameter of the LTCC design rules are used. The final dimensions of the via-based cavity are determined by using a tuning analysis of the HFSS full-wave simulator ( $L = 1.95 \text{ mm}$ ,  $W = 1.275 \text{ mm}$ ,  $H = 0.1 \text{ mm}$ ).

With the cavity size determined, microstrip lines are utilized as the feeding structure to excite the cavity via coupling slots that couple energy magnetically from the microstrip lines into the cavity. For a preliminary testing of the vertical inter-coupling of a three-pole cavity BPF, the input and output feedlines are placed on metal 1 and metal 4, respectively, as shown in Fig. 2. The coupling coefficient can be controlled by the location and size of the coupling slots etched on metal 2 and metal 3 in Fig. 2. The coupling slots are located a quarter of the cavity length from the sides and the slot length ("SL" in Fig. 2) is varied with the fixed slot width ( $\text{SW} \approx \lambda_g/4$  at 60.25 GHz) to achieve the desired frequency response [17].

To accurately estimate the unloaded quality factor ( $Q_u$ ), the weakly coupled cavity resonator [17] with a relatively small value of the slot length ["SL" in Fig. 3(d)] is implemented in

the HFSS simulator. The unloaded quality factor ( $Q_u$ ) can be extracted from the external quality factor ( $Q_{ext}$ ) and the loaded quality factor ( $Q_l$ ) using (2)–(4) [18]

$$Q_l = \frac{f_{res}}{\Delta f} \quad (2)$$

$$Q_{ext} = 10^{-[S_{21}(\text{dB})/20]} \cdot Q_l \quad (3)$$

$$Q_u = \left( \frac{1}{Q_l} - \frac{1}{Q_{ext}} \right)^{-1} \quad (4)$$

The simulated value of  $Q_u$  was calculated to be 623 at 60.25 GHz.

### B. Design of Three-Pole Cavity BPF

A vertically stacked LTCC three-pole cavity BPF is developed for 3-D integrated 59–64-GHz industrial, scientific, and medical (ISM) band transceiver front-end modules. The center frequencies of 60.25 and 62.75 GHz in the band are selected for the receiver channel (Rx channel) and the transmitter channel (Tx channel), respectively.

First, the cavity BPF for the Rx channel selection is designed with a 60.25-GHz center frequency, a <3-dB insertion loss, a 0.1-dB ripple, and a 4.15% ( $\approx 2.5$ -GHz) fractional bandwidth based on a Chebyshev low-pass prototype. The filter schematic is implemented with ten substrate layers of LTCC tape. Its 3-D overview, side view, top view of the feeding structure, and inter-resonator coupling structure are illustrated in Fig. 3(a)–(d), respectively. The top five substrate layers [substrate 1–5 in Fig. 3(b)] are occupied by the Rx filters, and the remaining layers are reserved for the antenna and RF active devices, which could be integrated into front-end modules. The microstrip lines on metal 1 and 6 are utilized as the feeding structure to excite the first and third cavities, respectively. Three identical cavity resonators [first, second, and third cavities in Fig. 3(b)] designed in Section II-A are vertically stacked and coupled through slots to achieve the desired frequency response with a high level of compactness. This filter is also an effective solution to connect the active devices on the top of the LTCC board and the antenna integrated on the back side.

Two external slots [see Fig. 3(b)] on metal layers 2 and 5 are dedicated to magnetically couple the energy from the I/O microstrip lines into the first and third cavity resonators, respectively. To maximize magnetic coupling by maximizing the current, the microstrip feedlines are terminated with a  $\lambda_g/4$  open stub beyond the center of each external slot. The fringing field generated by an open-end discontinuity can be modeled by an equivalent length of transmission line, which is determined to be approximately  $\lambda_g/20$ . Therefore, the optimum length of the stub is approximately  $\lambda_g/5$  [“MS” in Fig. 3(c)] [13], [17]. The position and size of the external slots are the main design parameters to provide the necessary  $Q_{ext}$ . The external quality factor ( $Q_{ext}$ ) that controls the insertion loss and ripple over the pass-band can be defined from the specifications as follows [19]:

$$Q_{ext} = \frac{g_i g_{i+1} f_{res}}{BW} \quad (5)$$

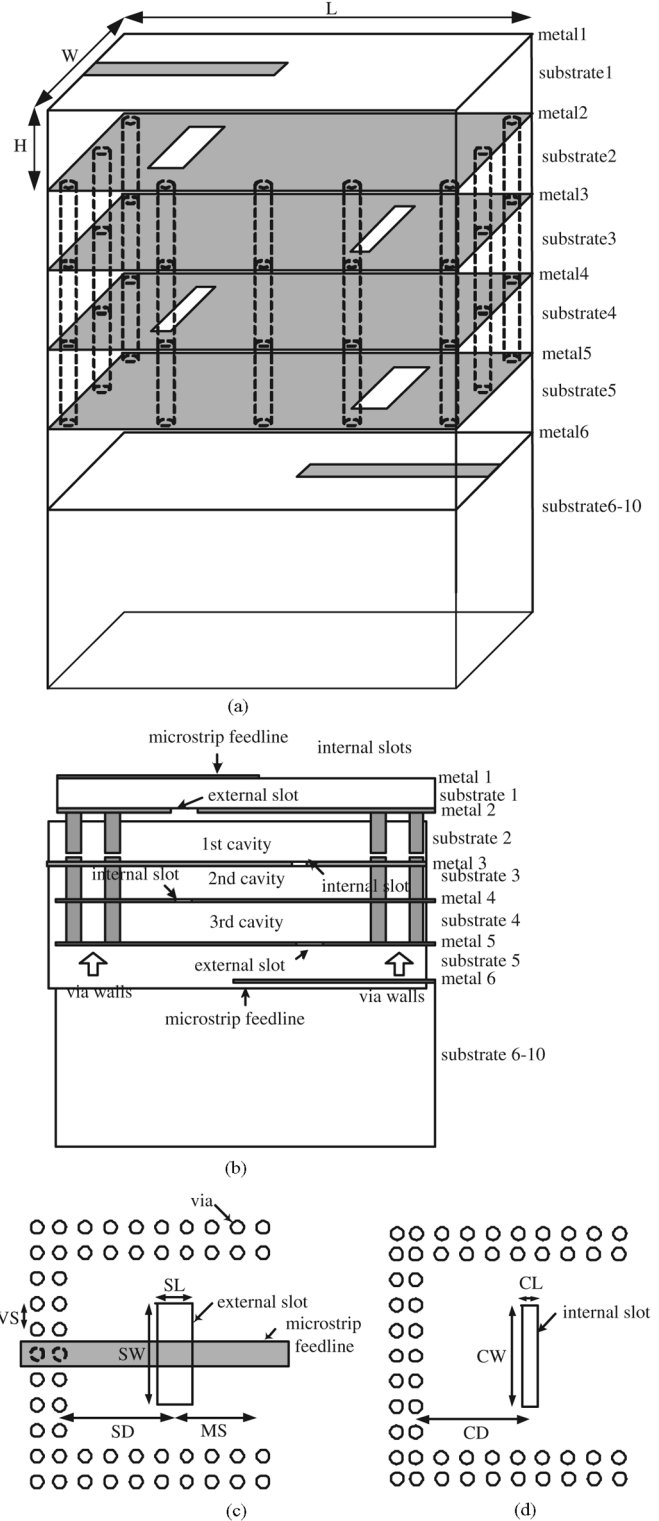


Fig. 3. (a) 3-D overview. (b) Side view of the vertically stacked three-pole cavity BPF. (c) Top view of the feeding structure. (d) Top view of the inter-resonator coupling structure.

where  $g_i$  are the element values of the low-pass prototype, BW is the bandwidth of the filter, and  $f_{res}$  is the resonant frequency.

The calculated  $Q_{ext}$  is 24.86. The external slot is initially positioned at  $L/4$  from the edge of the cavity, and the width [“SW” in Fig. 3(c)] of the slot is fixed to  $\lambda_g/4$ . The length [“SL” in

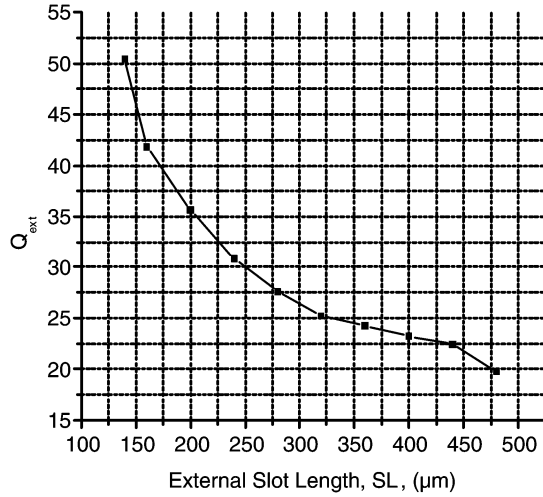


Fig. 4. External quality factor ( $Q_{\text{ext}}$ ) evaluated as a function of external slot length (SL).

Fig. 3(c)] of the slot is then tuned until the simulated  $Q_{\text{ext}}$  converges to the prototype requirement. Fig. 4 shows the relationship between the length variation of the external slots and the  $Q_{\text{ext}}$  extracted from the simulation using [19]

$$Q_{\text{ext}} = \frac{f_{\text{res}}}{\Delta f_{\pm 90^\circ}} \quad (6)$$

where  $\Delta f_{\pm 90^\circ}$  is the frequency difference between the  $\pm 90^\circ$  phase response of  $S_{11}$ .

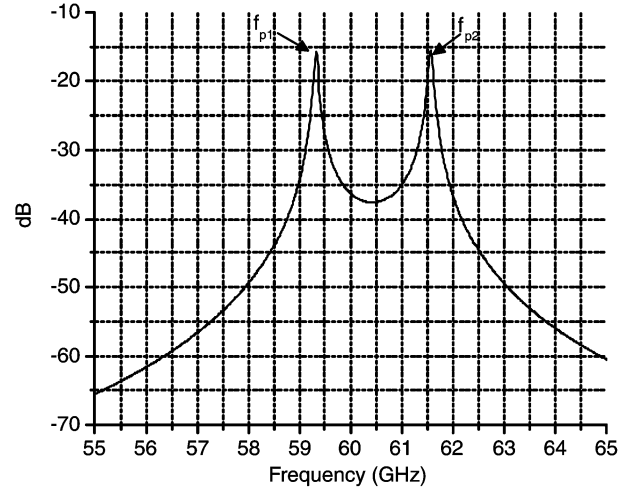
The latter internal slots on metal 3 and 4 [see Fig. 3(b)] are employed to couple energy from the first and third cavity resonators into the second resonator, and their design procedure is similar to that of the external slots. The internal slots are located a quarter of the cavity length from the sides. The desired inter-resonator coupling coefficients ( $k_{12} = k_{23} = 0.0381$ ) are obtained by [19]

$$k_{jj+1} = \frac{\text{BW}}{f_{\text{res}}} \sqrt{\frac{1}{g_j g_{j+1}}}. \quad (7)$$

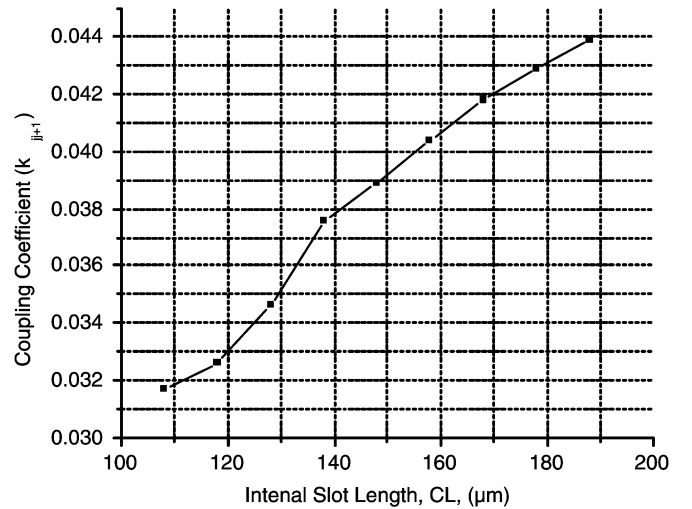
This desired prototype  $k_{jj+1}$  can be physically realized varying the slot length [“CL” in Fig. 3(d)] with a fixed slot width [ $\text{CW} \approx \lambda_g/4$  in Fig. 3(d)]. Full-wave simulations are employed to find the two characteristic frequencies ( $f_{p1}, f_{p2}$ ) that are the resonant frequencies in the transmission response of the coupled structure [19] and its plot versus frequency is shown in Fig. 5(a). These characteristic frequencies are associated to the inter-resonator coupling between the cavity resonators as follows [19]:

$$k_{jj+1} = \frac{f_{p2}^2 - f_{p1}^2}{f_{p2}^2 + f_{p1}^2}. \quad (8)$$

Fig. 5(b) shows the internal coupling as a function of the variation of the internal slot length [“CL” in Fig. 3(d)]. By adjusting



(a)



(b)

Fig. 5. (a) Two characteristic frequencies ( $f_{p1}, f_{p2}$ ) of the coupled cavities to calculate the internal coupling coefficients ( $k_{jj+1}$ ). (b) Inter-resonator coupling coefficient ( $k_{jj+1}$ ) as a function of internal slot length (CL).

the slot length, the optimal size of an internal slot can be determined for a given prototype value.

Using the initial dimensions of the external (SW, SL) and internal slot (CW, CL) size as the design variables, we optimized the design variables to realize the desired frequency response. The design can be fine tuned afterwards considering the minimum and maximum of the fabrication tolerances. The final variable values that match the desired frequency response can then be determined.

To allow on-wafer characterization using coplanar probes, the input and output probe pads have to be on the same layer, which requires an embedded microstrip line to CPW vertical transition at port 2. The vertical transition consists of five stacked signal vias penetrating through circular apertures [see Fig. 6(a)] on the ground planes (metals 2–5) and connecting an embedded microstrip line on metal 6 to a coplanar waveguide (CPW) measurement pads on metal 1. In order to match to the 50- $\Omega$  feedlines, the diameter of the circular apertures is optimized to be 0.57 mm for a signal via diameter of 130  $\mu\text{m}$ .

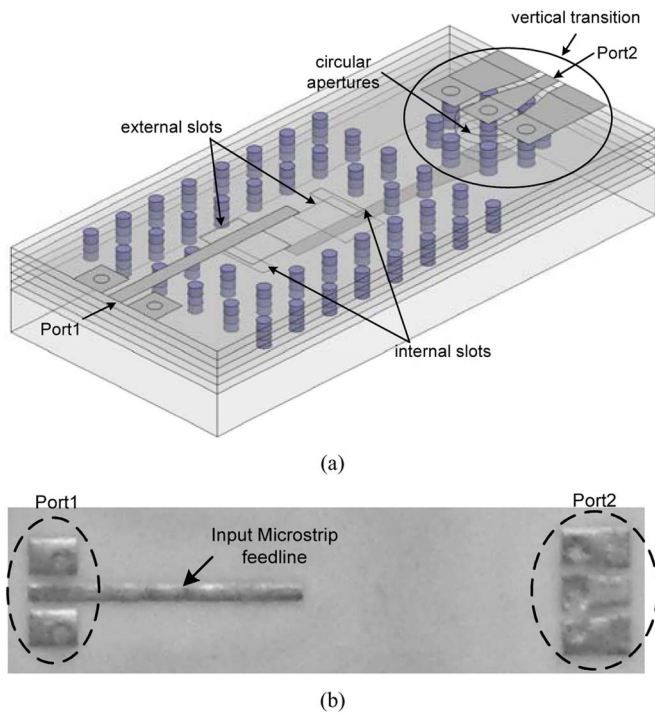


Fig. 6. (a) 3-D overview of vertically stacked three-pole cavity BPF with CPW pads and vertical transitions. (b) Cavity BPF fabricated on LTCC. (Color version available online at: <http://ieeexplore.ieee.org>.)

Eight shielding vias (two of shielding vias: connecting from metals 1 (CPW ground planes) to 5, six of shielding vias: connecting from metals 2 to 5) are also positioned around the apertures to achieve an optimum coaxial effect [20]. The number of shielding vias is determined with regard to the LTCC design rules.

The filters including CPW pads and a vertical transition were fabricated in LTCC by the Asahi Glass Company and measured on an HP8510C vector network analyzer using short-open-load-thru (SOLT) calibration. Fig. 6(a) depicts the 3-D overview of the complete structure that was simulated. The “Winical” software gives us the ability to deembed capacitance effects of CPW open pads and inductive effects of short pads from the measured  $S$ -parameters so that the loading shift effect could be negligible. Fig. 6(b) shows the photograph of the fabricated filter with CPW pads and a transition whose size is  $5.60 \times 3.17 \times 1 \text{ mm}^3$ . The cavity size is determined to be  $1.95 \times 1.284 \times 0.1 [L \times W \times H \text{ in Fig. 3(a)}] \text{ mm}^3$ .

Fig. 7(a) shows the comparison between the simulated and measured  $S$ -parameters of the three-pole vertically stacked BPF. The filter exhibits an insertion loss  $< 2.37 \text{ dB}$ , which is higher than the simulated value of  $< 1.87 \text{ dB}$ . The main source of this discrepancy might be caused by the radiation loss from the “thru” line that could not be deembedded because of the nature of SOLT calibration. The filter exhibits a 3-dB bandwidth approximately 3.5% ( $\approx 2 \text{ GHz}$ ) comparable to the simulated 3.82% ( $\approx 2.3 \text{ GHz}$ ). The narrower bandwidth in measurements might be due to the fabrication accuracy of the slot design that has been optimized for the original resonant frequencies and not for the shifted frequencies. The center frequency shift from 60.2 to 57.5 GHz might be attributed to

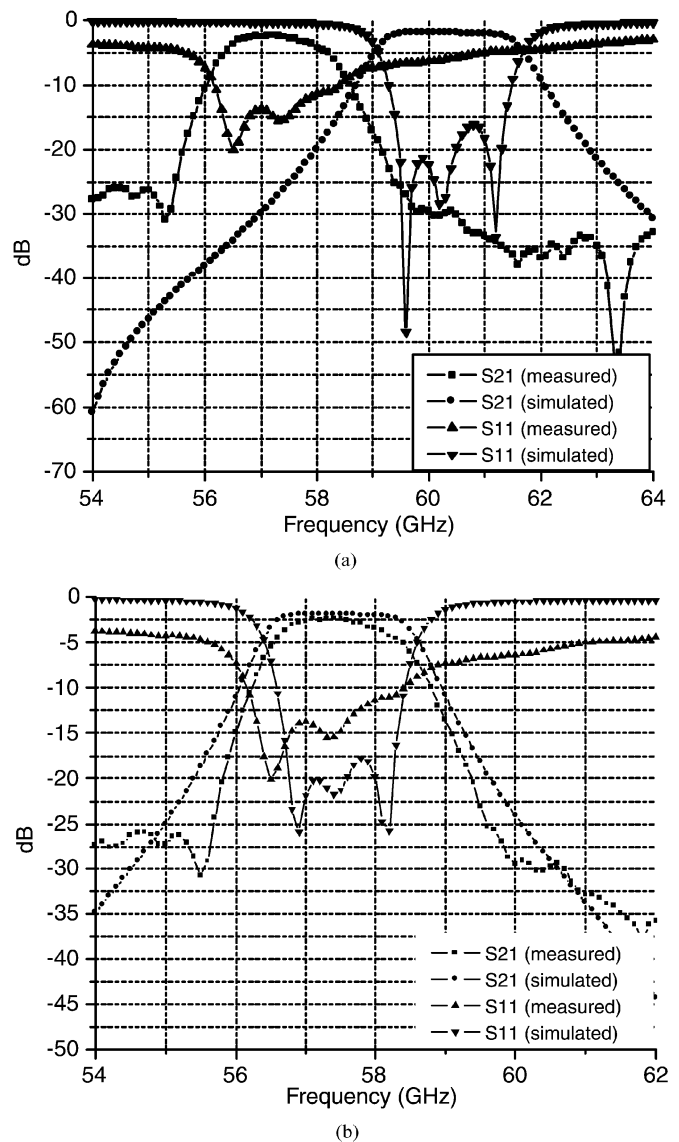


Fig. 7. Comparison between measured and simulated  $S$ -parameters ( $S_{11}$  and  $S_{21}$ ) of Rx three-pole cavity band filter. (a) Measurement versus simulation with  $\epsilon_r = 5.4$  and originally designed cavity size ( $1.95 \times 1.284 \times 0.1 \text{ mm}^3$ ). (b) Measurement versus simulation with  $\epsilon_r = 5.5$  and modified cavity size ( $2.048 \times 1.348 \times 0.1 \text{ mm}^3$ ).

the dielectric-constant variation at these high frequencies and the fabrication accuracy of vias positioning caused by  $XY$  shrinkage. The HFSS simulation is re-performed in terms of two aspects, which are as follows. 1) The dielectric constant of 5.4 was extracted using cavity resonator characterization techniques [21] at 35 GHz. The dielectric constant is expected to increase to 5.5 across 55–65 GHz [17]. 2) The tolerance of  $XY$  shrinkage is expected to be  $\pm 15\%$ .  $XY$  shrinkage specification was released after design tape out; thus, we could not have accounted it at the design stage.  $XY$  shrinkage can significantly affect the via positioning that is the major factor to determine the resonant frequency of a cavity filter. From our investigation, the averaged relative permittivity was evaluated to be 5.5 across 55–65 GHz [17], and the cavity size was modified to  $2.048 \times 1.348 \times 0.1 \text{ mm}^3$  with 5% of  $XY$  shrinkage effect. The exact coincidence between the measured center

TABLE I  
DESIGN PARAMETERS OF CAVITY RESONATORS

Design Parameters	1 <sup>st</sup> Channel	2 <sup>nd</sup> Channel
cavity length (L)	2.048	2.048
cavity width (W)	1.348	1.266
cavity height (H)	0.100	0.100
external slot width (SW)	0.628	0.621
external slot length (SL)	0.460	0.460
external slot position(SD)	0.417	0.417
internal slot width (CW)	0.558	0.551
internal slot length (CL)	0.138	0.138
internal slot position(CD)	0.417	0.417
open stub length (MS)	0.571	0.571

frequency (57.5 GHz) and the simulated frequency (57.5 GHz) is observed in Fig. 7(b). All design parameters for the modified Rx filter are summarized in Table I.

The same techniques were then applied to the design of the cavity BPF for the Tx channel (61.5–64 GHz). The Chebyshev prototype filter was designed for a center frequency of 62.75 GHz, a <3-dB insertion loss, a 0.1-dB band ripple, and a 3.98% 3-dB bandwidth. To meet the specified center frequency specs, the cavity width ( $W$ ) was decreased. The cavity size was then determined to be  $1.95 \times 1.206 \times 0.1$  [ $L \times W \times H$  in Fig. 3(a)]  $\text{mm}^3$ . The external and internal coupling slot sizes are used as the main design parameters to obtain the desired external quality factors and coupling coefficients, respectively.

The measured results of the Tx filter exhibit an insertion loss of 2.39 dB with a 3-dB bandwidth of 3.33% ( $\sim 2$  GHz) at the center frequency of 59.9 GHz. The center frequency is downshifted approximately 2.72 GHz, which is similar to the Rx filter. A new theoretical simulation was performed with  $\epsilon_r = 5.5$  and the 5% increase in the volume of cavity ( $2.048 \times 1.266 \times 0.1 \text{ mm}^3$ ), and the measured and simulated results are presented in Fig. 8. The simulation showed a minimum insertion loss of 1.97 dB with a slightly increased 3-dB bandwidth of 4% ( $\sim 2.4$  GHz). The center frequency of the simulated filter was 59.9 GHz. The center frequency shift is consistent through all devices using this LTCC process because of the fabrication tolerances mentioned. All design parameters for the modified Tx filter are summarized in Table I.

### III. DUPLEXER (60/62.8 GHz)

The development of a 3-D fully integrated compact duplexer is crucial in a 3-D 59–64-GHz ISM band transceiver front-end module to isolate the power transmit stage from a sensitive receiving stage sharing a common antenna. A low insertion loss in the transmitter and receiver paths is the most fundamental requirement because a low loss enhances the sensitivity of the receiver and prevents the excessive power consumption in the transmitter. In addition, the high channel-to-channel isolation must be accomplished by minimizing the electrical coupling level between the transmitter and receiver.

We have designed and fabricated one duplexer consisting of the two resonant three-pole cavity filters developed in Section II and one microstrip T-junction, which connects the two

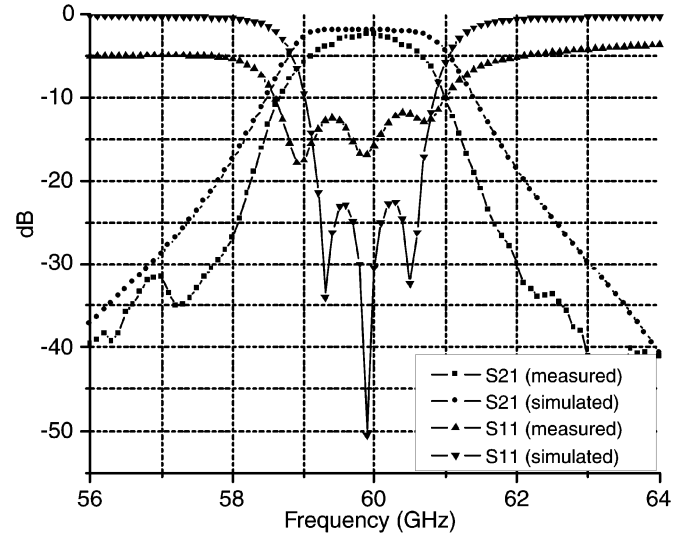


Fig. 8. Comparison between measured and simulated  $S$ -parameters ( $S_{11}$  and  $S_{21}$ ) of Tx three-pole cavity band filter (simulation with  $\epsilon_r = 5.5$  and modified cavity size ( $2.048 \times 1.266 \times 0.1 \text{ mm}^3$ ) versus measurement).

filters and the common input reserved for an antenna. The two channels of the duplexer are centered at 60 GHz for the Rx channel (first channel) and 62.8 GHz for the Tx channel (second channel). The insertion loss <3 dB and bandwidths  $\approx 2.5$  GHz are desired for both channels. The 3-D overview and top view of the duplexer including the vertical transitions and CPW pads are illustrated in Fig. 9(a) and (b), respectively. The duplexer that dominates five substrate layers is implemented into a module with ten layers of LTCC tape. The remaining five substrate layers are used for burying RF circuitry that includes the antenna and integrated active devices. The 60-GHz cavity filter occupies the left portion of the duplexer and 62.8-GHz cavity filter occupies the right portion, as shown in Fig. 9(a) and (b). The same configurations of the 3-D cavity filters [see Fig. 3] developed in Section II are employed to the duplexer except from a slight modification of the cavity widths ( $W_1$  and  $W_2$  in Fig. 9) corresponding to the resonant frequencies of two channels. The modification was necessary to achieve the high level of channel-to-channel isolation that is aimed to be more than 30 dB over operating frequency bands. The cavity sizes are determined to be  $1.95 \times 1.29 \times 0.1 \text{ mm}^3$  for the first channel and  $1.95 \times 1.201 \times 0.1 \text{ mm}^3$  for the second channel. The spacing of two filters is 1.6 mm.

The lengths of the microstrip lines [ $T_1$  and  $T_2$  in Fig. 9(b)] connecting the T-junction to the Rx and Tx filters are the most important design parameters to achieve the good isolation between two channels. First we set up  $T_1$  and  $T_2$  to be equal to a half guided wavelength at the resonant frequencies of the first channel and second channel filters accordingly. In our case, one guided wavelength is utilized as the initial value of  $T_1$  and  $T_2$  since a length equal to one half guided wavelength would cause an overlap between two filters. The length of  $T_1$  is then optimized to reflect an open circuit at the resonant frequency of the second channel in the HFSS simulator. The length  $T_2$  is also optimized against the first channel in the same way as applied to  $T_1$ :  $T_1 = 2.251 \text{ mm}$  and  $T_2 = 2.135 \text{ mm}$ . The optimized lengths are compensated for the fringing effects of the open stubs.

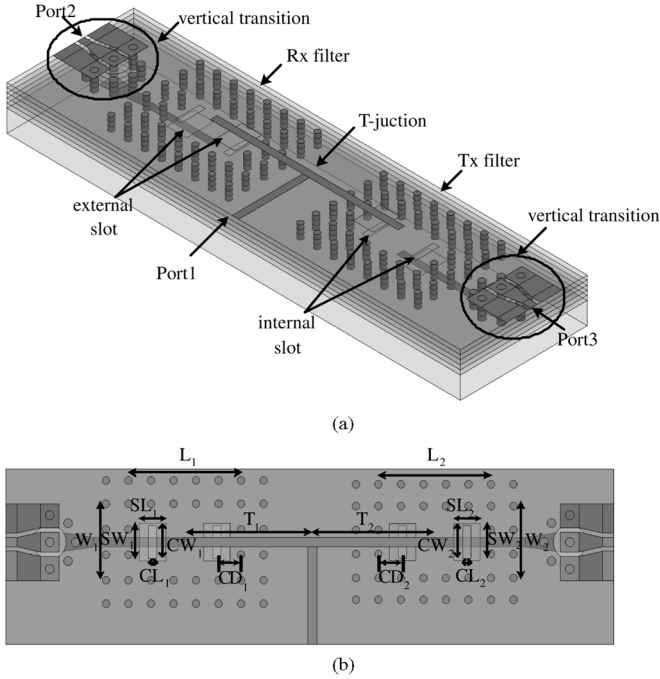


Fig. 9. (a) 3-D overview and (b) top view of the proposed LTCC cavity duplexers using microstrip T-junction.

Fig. 10(a) and (b) shows the measured and simulated insertion-loss results of the LTCC duplexer for the first channel and second channel, respectively. In the simulation, the higher dielectric constant ( $\epsilon_r = 5.5$ ) and 5% increase in the volume of cavities were taken into account based on the investigation in Section II. All design parameters depicted in Fig. 9(b) for the modified duplexer are summarized in Table II.

The Rx filter exhibits an insertion loss  $< 2.22$  dB, which is slightly higher than the simulated value of 2.07 dB, and a 3-dB bandwidth of approximately 2.4 GHz ( $\sim 4.20\%$ ) at the center frequency of 57.2 GHz compared to a simulated value of a 3-dB bandwidth of 2.7 GHz ( $\sim 4.71\%$ ) at the center frequency of 57.25 GHz, as shown in Fig. 10(a). In Fig. 10(b), the insertion loss for the second channel is measured to be 2.48 dB, which is very close to the simulated value of 2.46 dB. The Tx measurement shows a narrower 3-dB bandwidth of 1.6 GHz ( $\sim 2.66\%$ ) at the center frequency of 60.1 GHz than the simulated 3-dB bandwidth of 2.6 GHz ( $\sim 4.32\%$ ) at the center frequency of 60.15 GHz. The discrepancy between the measured and simulated insertion loss could be attributed to the metal loss from the roughness of screen printing on LTCC. The fabrication accuracy of the layer alignment could be responsible for the narrower bandwidth in the measurement because it could affect the external slots position that is a major factor to decide the bandwidth. Fig. 11(a) and (b) shows the measured and simulated return loss and the measured channel-to-channel isolation, respectively. The measured isolation is better than 35.2 dB across the first band and better than 38.4 dB across the second band. The summary of cavity duplexer results is presented in Table III.

#### IV. INTEGRATION (FILTERS AND ANTENNA)

The optimal integration of antennas and filters into a 3-D 59–64 GHz transceiver front-end module is significantly de-

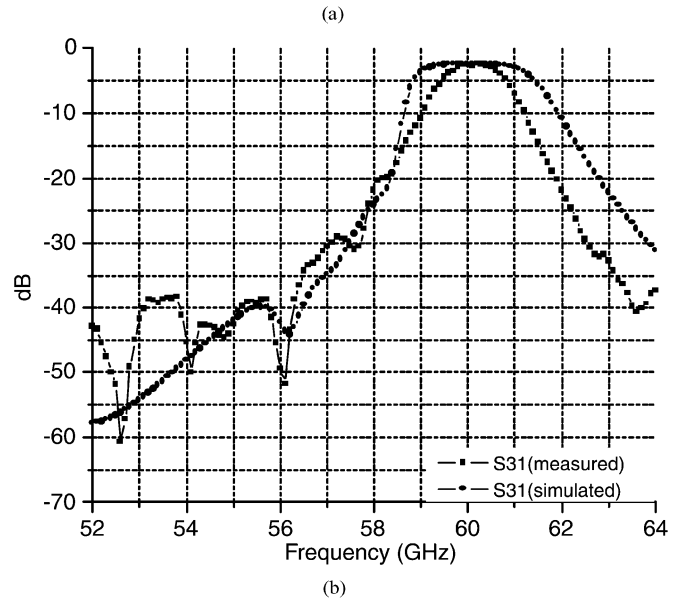
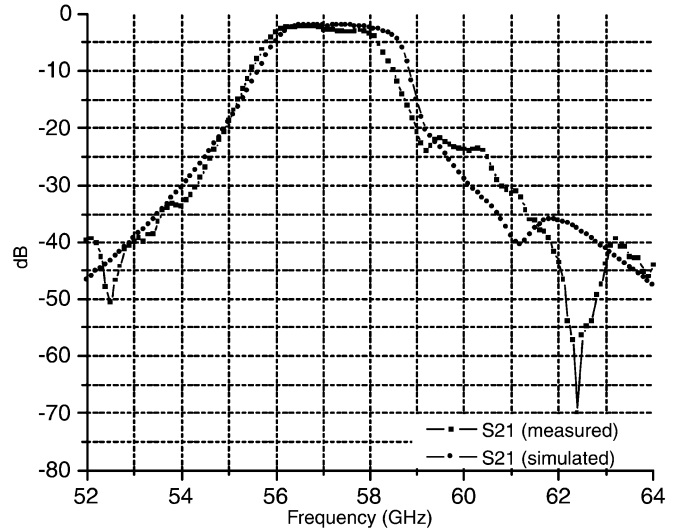


Fig. 10. (a)  $S_{21}$  response in the first channel of the duplexer [measurement versus simulation with  $\epsilon_r = 5.5$  and modified cavity size ( $2.048 \times 1.354 \times 0.1$  mm<sup>3</sup>)]. (b)  $S_{31}$  response in the second channel of the duplexer [measurement versus simulation with  $\epsilon_r = 5.5$  and modified cavity size ( $2.048 \times 1.261 \times 0.1$  mm<sup>3</sup>)].

TABLE II  
DESIGN PARAMETERS OF CAVITY DUPLEXERS

1 <sup>st</sup> Channel		2 <sup>nd</sup> Channel	
Design Parameters	mm	Design Parameters	mm
cavity length ( $L_1$ )	2.048	cavity length ( $L_2$ )	2.048
cavity width ( $W_1$ )	1.354	cavity width ( $W_2$ )	1.261
each cavity height (H)	0.100	each cavity height (H)	0.100
ex. slot width ( $SW_1$ )	0.628	ex. slot width ( $SW_2$ )	0.621
ex. slot length ( $SL_1$ )	0.460	ex. slot length ( $SL_2$ )	0.460
ex. slot position ( $SD_1$ )	0.417	ex. slot position ( $SD_2$ )	0.417
in. slot width ( $CW_1$ )	0.558	in. slot width ( $CW_2$ )	0.551
in. slot length ( $CL_1$ )	0.138	in. slot length ( $CL_2$ )	0.138
in. slot position ( $CD_1$ )	0.417	in. slot position ( $CD_2$ )	0.417
microstrip length ( $T_1$ )	2.251	microstrip length ( $T_2$ )	2.135

sirable since it not only reduces cost, size, and system complexity, but also achieves a high level of band selectivity and

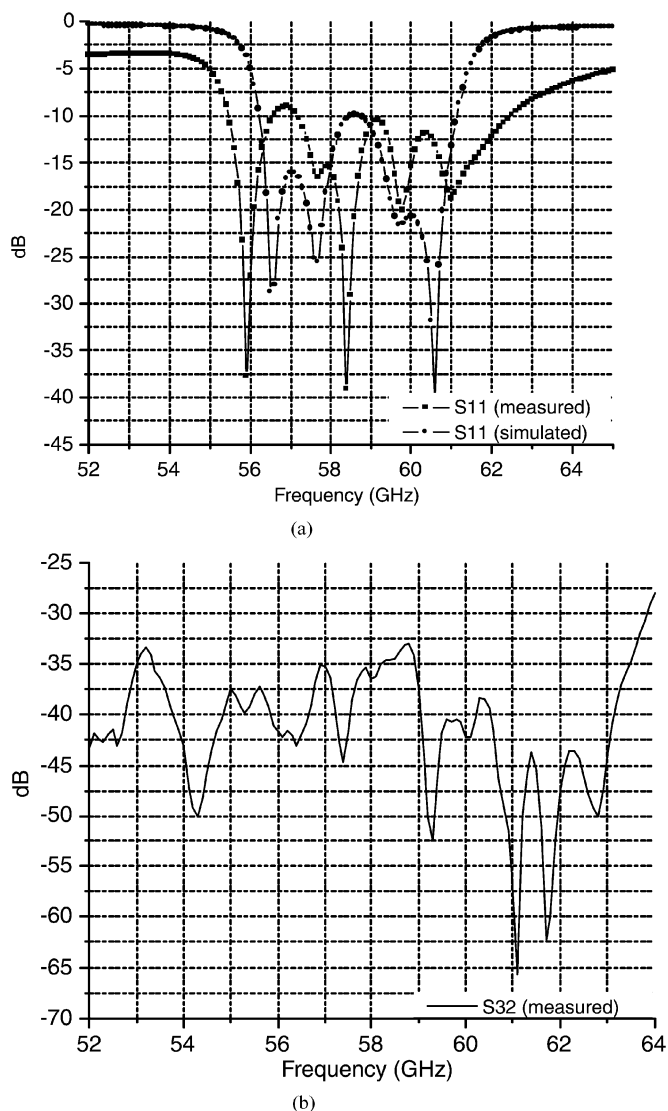


Fig. 11. (a)  $S_{11}$  response of the duplexer (measurement versus simulation with  $\epsilon_r = 5.5$  and modified cavity sizes). (b) Measured  $S_{32}$  response in the isolation between the first and second channels.

TABLE III  
PERFORMANCE OF CAVITY DUPLEXERS

Design Parameters	1 <sup>st</sup> Channel		2 <sup>nd</sup> Channel	
	Sim.	Meas.	Sim.	Meas.
Insertion Loss (dB)	>2.07	>2.22	>2.46	>2.48
Bandwidth (%)	4.71	4.20	4.32	2.66
Return Loss (dB)	>16	>9	>20.67	>11.84
Center Frequency (GHz)	57.25	57.2	60.15	60.1
Isolation (dB)	>23.49	>35.18	>23.48	>38.36

spurious suppression. Although cost, electrical performance, integration density, and packaging capability are often at odds in RF front-end designs, the performance of the module can be significantly improved by employing the 3-D integration of filters and antennas using the flexibility of multilayer architecture on LTCC. Here, the fully integrated Rx and Tx filters and the dual-polarized antenna that covers Rx (first) and Tx (second) channels are proposed employing the presented designs of the

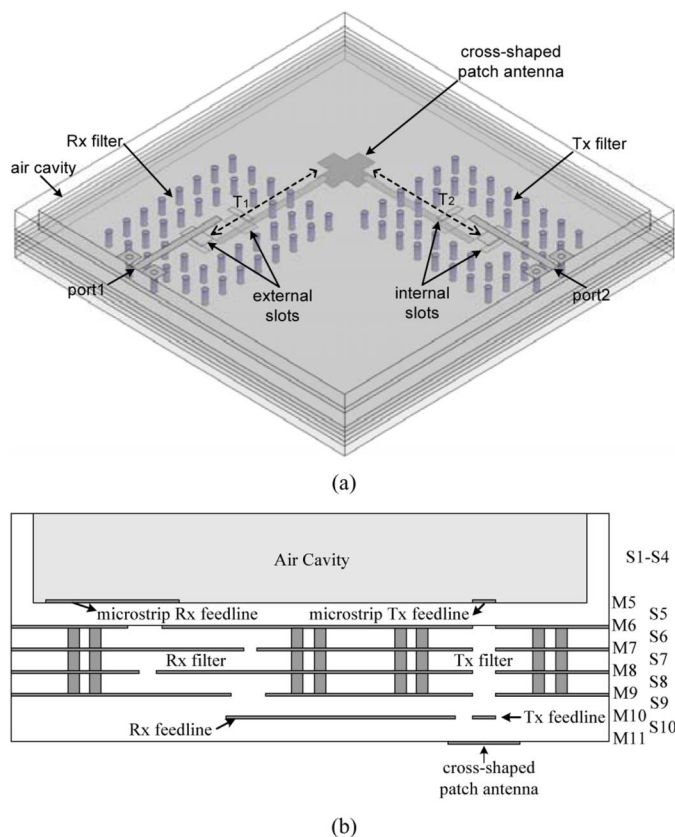


Fig. 12. (a) 3-D overview and (b) cross-sectional view of the 3-D integration of the filters and antennas using LTCC multilayer technologies. (Color version available online at: <http://ieeexplore.ieee.org>.)

filters. The filters' matching ( $>10$  dB) toward the antenna and the isolation ( $>45$  dB) between Rx and Tx paths comprise the excellent features of this compact 3-D design. The stringent demand of high isolation between two channels induces the advanced design of a duplexer and an antenna as a fully integrated function for the V-band front-end module.

The 3-D overview and the cross-sectional view of the topology chosen for the integration are shown in Fig. 12(a) and (b), respectively. A cross-shaped patch antenna [4] designed to cover two bands between 59–64 GHz (first channel: 59–61.5 GHz, second channel: 61.75–64 GHz) is located at the most bottom metal layer [M11 in Fig. 12(b)]. The cross-shaped geometry was utilized to decrease the cross-polarization, which contributes to unwanted sidelobes in the radiation pattern [4]. The cross-channel isolation can be improved by receiving and transmitting signals in two orthogonal polarizations. The feedlines and patch are implemented into different vertical metal layers (M10 and M11, respectively), and then the end-gap capacitive coupling is realized by overlapping the end of the embedded microstrip feedlines and the patch. The overlap distance for the Rx and Tx feedline is approximately 0.029 and 0.03 mm, respectively. The common ground plane for the feedlines and the patch is placed one layer above the feedlines, as shown in Fig. 12(b). The two antenna feedlines [Rx feedline and Tx feedline in Fig. 12(b)] are commonly utilized as the filters' feedlines that excite the Rx and Tx filters accordingly through external slots placed at M9 in Fig. 12(b). The lengths

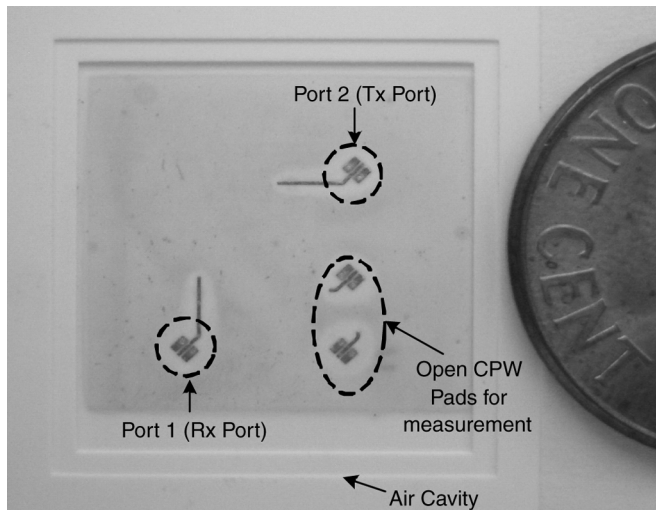
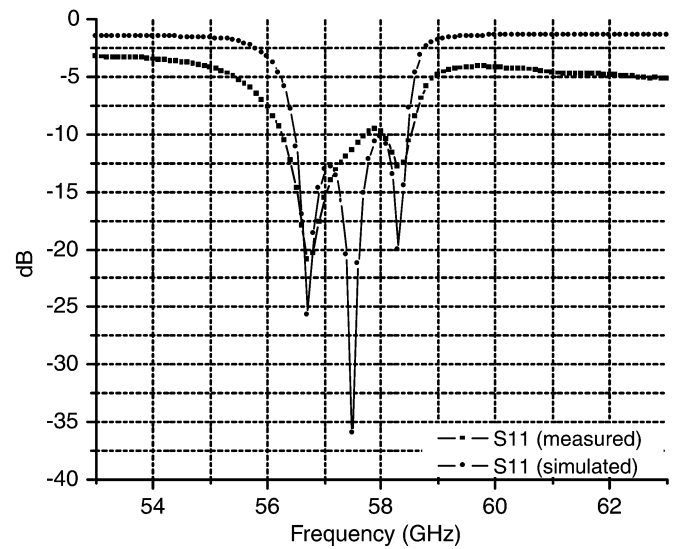


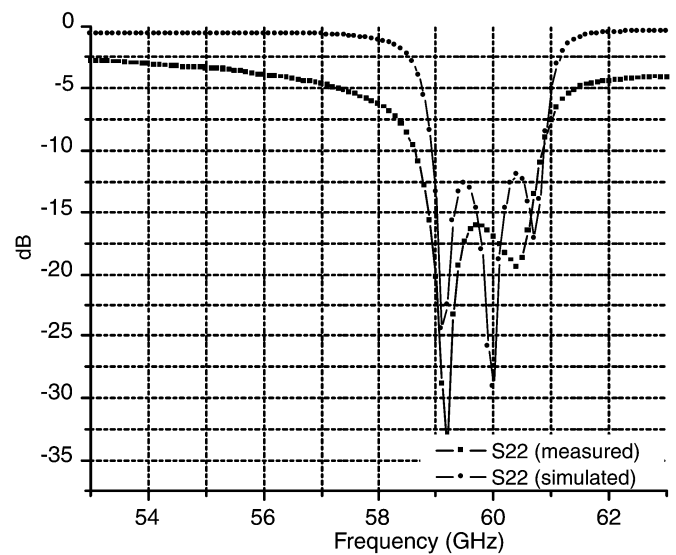
Fig. 13. Top view of the integrated function of Rx/Tx cavity filters and cross-shaped patch antenna with the air cavity top.

of Rx and Tx feedlines [ $T_1$  and  $T_2$  in Fig. 12(a)] connecting the cross-shaped antenna to the Rx and Tx filters, respectively, are initially set up to be one guided wavelength at the corresponding center frequency of each channel and are optimized using the HFSS simulator in the way discussed in Section III ( $T_1$ : 2.745 mm,  $T_2$ : 2.650 mm). The 3-D Rx and Tx filters (see Fig. 3) designed in Section II are directly integrated to the antenna, exploiting the design parameters listed in Table I. The integrated filters and antenna function occupies six substrate layers (S5–S10: 600  $\mu\text{m}$ ). The remaining four substrate layers [S1–S4 in Fig. 12(b)] are dedicated to the air cavities reserved for burying RF active devices (RF receiver and transmitter MMICs) that are located beneath the antenna on purpose not to interfere with the antenna performance and to be highly integrated with the microstrip (Rx/Tx) feedlines, leading to significant volume reduction, as shown in Fig. 12. The cavities are fabricated removing the inner portion of the LTCC material outlined by the successively punched vias. The deformation factor of a cavity that is defined to be the physical depth difference between the designed one and the fabricated one is stable in the LTCC process when the depth of the cavity is less than two-thirds of the height of the board. Since we have chosen the air cavity depth of 400  $\mu\text{m}$ , which is suitable for Rx/Tx MMIC chipsets, to enable the full integration of MMICs and passive front-end components, we can limit the fabrication tolerances effect of an air cavity to the other integrated circuitries. Fig. 13 shows a photograph of the integrated device, which is equipped with one air cavity at the top layers. The device occupies an area of  $7.94 \times 7.82 \times 1 \text{ mm}^3$  including the CPW measurement pads.

Fig. 14 shows the simulated and measured return losses ( $S_{11}/S_{22}$ ) of the integrated structure. In the simulation, the higher dielectric constant ( $\epsilon_r = 5.5$ ) and 5% increase in the volume of cavity were applied. It is observed from the first channel that the 10-dB return-loss bandwidth is approximately 2.4 GHz ( $\sim 4.18\%$ ) at the center frequency of 57.45 GHz that is slightly wider than the simulation of 2.1 GHz ( $\sim 3.65\%$ ) at



(a)



(b)

Fig. 14. Comparison between measured and simulated return loss. (a)  $S_{11}$  of the first channel. (b)  $S_{22}$  of the second channel.

57.5 GHz, as shown in Fig. 14(a). The slightly increased bandwidth may be attributed to parasitic radiation from the feedlines or the measurement pads. In Fig. 14(b), the return-loss measurement from the second channel also exhibits a wider bandwidth of 2.3 GHz ( $\sim 3.84\%$ ) at the center frequency of 59.85 GHz compared to the simulated value of 2.1 GHz ( $\sim 3.51\%$ ) at that of 59.9 GHz. The measured channel-to-channel isolation is illustrated in Fig. 15. The measured isolation is better than 49.1 dB across the first band (56.2–58.6 GHz) and better than 51.9 dB across the second band (58.4–60.7 GHz), which is significantly improved in comparison with the cavity duplexer using the T-junction presented in Section III.

## V. CONCLUSION

We have successfully demonstrated the fully integrated 3-D cavity filters/duplexers and antennas as a SOP passive front-end solution of the V-band LTCC transceiver module. The advanced

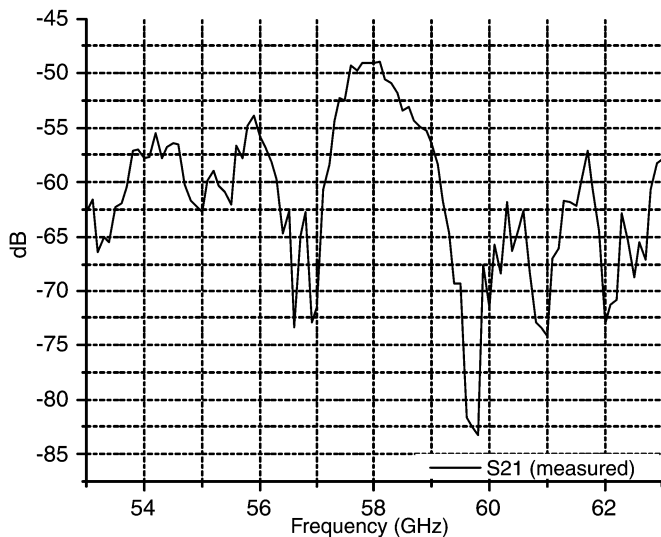


Fig. 15. Measured channel-to-channel isolation ( $S_{21}$ ) of the integrated structure.

design of high-performance 60-GHz passive building blocks and their compact 3-D integration using the very mature fabrication capability of LTCC has been reported with high integration potential. Vertically stacked 3-D low-loss cavity BPFs have been developed for Rx and Tx channels to realize a compact duplexer integrated into a 3-D V-band transceiver module. Excellent performance for both channels has been observed with low insertion loss such as  $< 2.37$  and  $< 2.39$  dB, respectively. The resonant frequency downshift about 2.7 GHz has been observed through all devices fabricated on this LTCC process. The fabrication tolerances such as the dielectric constant variation (5.5 versus 5.4) at these high frequencies and the accuracy of vias positioning caused by XY shrinkage ( $\sim 5\%$ ) have been interpreted as major factors for these phenomena and considered in the simulations of the rest devices. The duplexer consisting of the developed cavity filters were then demonstrated with the specific passband characteristics (4.2% at 57.2 GHz, 2.66% at 60.1 GHz), low insertion loss (2.22/2.48 dB), and a high level of channel-to-channel isolation (35.2/38.4 dB). Finally, the fully integrated functions of Rx and Tx filters and the dual-polarized antenna that covers Rx and Tx channels have been proposed employing a novel 3-D deployment of embedded components with an air cavity. The excellent overall performance of the integration has been verified through 10-dB BW of 2.4 GHz ( $\sim 4.18\%$ ) at 57.45 GHz and 2.3 GHz ( $\sim 3.84\%$ ) at 59.85 GHz and the measure isolation better than 49 dB across the Rx band and better than 51.9 dB across the Tx band. The proposed 3-D integrated functions can be easily integrated with Rx/Tx MMICs to realize an LTCC V-band transceiver front-end module.

#### ACKNOWLEDGMENT

The authors would like to thank Prof. J. Papapolymerou, Georgia Institute of Technology, Atlanta, for his insightful comments on resonator issues.

#### REFERENCES

- [1] C. H. Doan, S. Emami, D. A. Sobel, A. M. Niknejad, and R. W. Brodersen, "Design considerations for 60 GHz CMOS radios," *IEEE Commun. Mag.*, vol. 42, no. 12, pp. 132–140, Dec. 2004.
- [2] K. Kornegay, "60 GHz radio design challenges," in *GaAs IC Symp. Dig.*, San Diego, CA, Nov. 2003, pp. 89–92.
- [3] Y. Takimoto, H. Yatsuka, A. Inoue, T. Yokoyama, T. Aoyagi, K. Ohata, T. Saito, T. Negishi, and N. Okubo, in *IEEE MTT-S Int. Microw. Symp. Dig.*, San Francisco, CA, Jun. 1996, pp. 509–512.
- [4] J.-H. Lee, G. DeJean, S. Sarkar, S. Pintel, K. Lim, J. Papapolymerou, J. Laskar, and M. M. Tentzeris, "Highly integrated millimeter-wave passive components using 3-D LTCC system-on-package (SOP) technology," *IEEE Trans. Microw. Theory Tech.*, vol. 53, no. 6, pp. 2220–2229, Jun. 2005.
- [5] Y. C. Lee, W.-I. Chang, Y. H. Cho, and C. S. Park, "A very compact 60 GHz transmitter integrating GaAs MMICs on LTCC passive circuits for wireless terminals applications," in *IEEE MTT-S Int. Microw. Symp. Dig.*, Fort Worth, TX, Oct. 2004, pp. 313–316.
- [6] K. Ohata, T. Inoue, M. Funabashi, A. Inoue, Y. Takimoto, T. Kuwabara, S. Shinozaki, K. Maruhashi, K. Hosaya, and H. Nagai, "60-GHz-band ultra-miniature monolithic T/R modules for multimedia wireless communication systems," *IEEE Trans. Microw. Theory Tech.*, vol. 44, no. 12, pp. 2354–2360, Dec. 1996.
- [7] K. Ohata, K. Maruhashi, M. Ito, S. Kishimoto, K. Ikuina, T. Hashiguchi, K. Ikeda, and N. Takahashi, "1.25 Gbps wireless gigabit ethernet link at 60 GHz-band," in *IEEE MTT-S Int. Microw. Symp. Dig.*, Philadelphia, PA, Jun. 2003, pp. 373–376.
- [8] J. Mizoe, S. Amano, T. Kuwabara, T. Kaneko, K. Wada, A. Kato, K. Sato, and M. Fujise, "Miniature 60 GHz transmitter/receiver modules on AlN multi-layer high temperature co-fired ceramic," in *IEEE MTT-S Int. Microw. Symp. Dig.*, Anaheim, CA, Jun. 1999, pp. 475–478.
- [9] F. Kuroki, Y. Murata, and T. Yoneyama, "Filter-based NRD-guide duplexer with low loss and high isolation at 60 GHz," *Electron. Lett.*, vol. 40, no. 13, pp. 808–810, Jun. 2004.
- [10] T. Matsuda, J. Tsutsumi, S. Inoue, Y. Iwamoto, and Y. Sato, "High-frequency SAW duplexer with low-loss and steep cut-off characteristics," in *IEEE Ultrason. Symp.*, Munich, Germany, Oct. 2002, pp. 71–76.
- [11] F. M. Pitschi, J. E. Kiwitt, B. Bader, and K. C. Wagner, "On the design of an FBAR PCS duplexer in LTCC chip-sized package," in *IEEE Ultrason. Symp.*, Montreal, QC, Canada, Aug. 2004, pp. 1525–1528.
- [12] S. Marksteiner, M. Handtmann, H.-J. Timme, and R. Aigner, "A miniature BAW duplexer using flip-chip on LTCC," in *IEEE Ultrason. Symp.*, Honolulu, HI, Oct. 2003, pp. 1794–1797.
- [13] L. Harle and L. P. B. Katehi, "A vertically integrated micromachined filter," *IEEE Trans. Microw. Theory Tech.*, vol. 50, no. 9, pp. 2063–2068, Sep. 2002.
- [14] J.-H. Lee, N. Kidera, S. Pintel, J. Papapolymerou, J. Laskar, and M. M. Tentzeris, "A highly integrated 3-D millimeter-wave filter using LTCC system-on-package (SOP) technology for V-band WLAN gigabit wireless systems," in *Proc. 17th Asia-Pacific Microw. Conf.*, Suzhou, China, 2005, pp. 3–5.
- [15] R. E. Collin, *Foundations for Microwave Engineering*. New York: McGraw-Hill, 1992.
- [16] M. J. Hill, R. W. Ziolkowski, and J. Papapolymerou, "Simulated and measured results from a Duroid-based planar MBG cavity resonator filter," *IEEE Microw. Wireless Compon. Lett.*, vol. 10, no. 12, pp. 528–530, Dec. 2000.
- [17] J.-H. Lee, S. Pintel, J. Papapolymerou, J. Laskar, and M. M. Tentzeris, "Low loss LTCC cavity filters using system-on-package technology at 60 GHz," *IEEE Trans. Microw. Theory Tech.*, vol. 53, no. 12, pp. 231–244, Dec. 2005.
- [18] D. M. Pozar, *Microwave Engineering*, 2nd ed. New York: Wiley, 1998.
- [19] J.-S. Hong and M. J. Lancaster, *Microstrip Filters for RF/Microwave Applications*. New York: Wiley, 2001.
- [20] J. Heyen, A. Gordiyenko, P. Heide, and A. F. Jacob, "Vertical feedthroughs for millimeter-wave LTCC modules," in *IEEE Eur. Microw. Conf.*, Munich, Germany, Oct. 2003, pp. 411–414.
- [21] D. C. Thomson, O. Tantot, H. Jallageas, G. E. Ponchak, M. M. Tentzeris, and J. Papapolymerou, "Characterization of liquid crystal polymer (LCP) material and transmission lines on LCP substrates from 30 to 110 GHz," *IEEE Trans. Microw. Theory Tech.*, vol. 52, no. 4, pp. 1343–1352, Apr. 2004.



**Jong-Hoon Lee** (S'98) received the B.S. degree in electrical engineering from Pennsylvania State University, University Park, in 2001, the M.S. degree from the Georgia Institute of Technology, Atlanta, in 2004, and is currently working toward the Ph.D. degree in electrical and computer engineering at the Georgia Institute of Technology.

He is a member of the Georgia Institute of Technology ATHENA Research Group, National Science Foundation (NSF) Packaging Research Center, and the Georgia Electronic Design Center, Atlanta. He

has authored or coauthored over 27 papers in referred journals and conference proceedings. His research interests are packaging technology for microwave/millimeter-wave systems, passive/active circuits for RF/wireless systems, and digital signal processing (DSP)-based predictor to improve the computational efficiency of the simulation. He is currently involved in research and development of LTCC SOP modules for millimeter-wave wireless systems and the high-frequency material characterization for millimeter-wave 3-D modules.



**Nobutaka Kidera** received the B.S and M.S. degrees in electrical engineering from Kyushu University, Fukuoka, Japan in 1992 and 1994, respectively.

In 1994, he joined the Asahi Glass Company Ltd., Yokohama, Japan, where he has engaged in research and development on electrically conductive materials, wiring circuits and antennas for automotive applications. He is currently engaged in research on RF embedded passives using LTCC for microwave applications. From 2003 to 2005, he was a Visiting Scholar with the Microwave Application Group,

Georgia Electronic Design Center, Georgia Institute of Technology, Atlanta.

Mr. Kidera is a member of the International Microelectronics and Packaging Society (IMAPS).



**Gerald DeJean** (S'03) received the Bachelor's of Science degree in electrical engineering (with high honors) from Michigan State University, East Lansing, in 2000, and is currently working toward the Ph.D. degree in electrical engineering at the Georgia Institute of Technology, Atlanta.

He is currently with the ATHENA Research Group, Georgia Institute of Technology. He is also a member of the Georgia Electronic Design Center and the National Science Foundation (NSF) Packaging Research Center. His current research interests

include the design of compact antennas for integration into 3-D transceiver design, integration of antennas on multilayer substrates, equivalent-circuit modeling of antennas, and RF packaging and design.



**Stéphane Pinel** (M'05) received the B.S. degree from Paul Sabatier University, Toulouse, France, in 1997, and the Ph.D. degree in microelectronics and microsystems (with highest honors) from the Laboratoire d'Analyse et d'Architecture des Systèmes, Centre National de la Recherche Scientifique, Toulouse, France, in 2000.

For three years, he has been involved with an Ultra-Thin Chip Stacking (UTCS) European Project. He is currently a Research Engineer with the Microwaves Applications Group, Georgia Institute of Technology,

Atlanta. He has authored or coauthored over 110 journal and proceeding papers, two book chapters, and numerous invited talks. He holds four patents/invention disclosures. His research interests include advanced 3-D integration and pack-

aging technologies, RF and millimeter-waves embedded passives design using organic and ceramic material, RF microelectromechanical systems (MEMS) and micromachining techniques, SOP for RF front-end modules, and system-on-insulator (SOI) RF circuit design.

Dr. Pinel has participated and organized numerous workshops. He was the recipient of the First Prize Award presented at the 1998 Society of Electronic and Electro-technique (SEE), the Second Prize Award presented by the 1999 International Microelectronics and Packaging Society (IMAPS), and the Best Paper Award presented at the 2002 International Conference on Microwave and Millimeter-Wave Technology, Beijing, China.



**Joy Laskar** (S'84-M'85-SM'02-F'05) received the B.S. degree (with highest honors) in computer engineering with math/physics minors from Clemson University, Clemson, SC, in 1985, and the M.S. and Ph.D. degrees in electrical engineering from the University of Illinois at Urbana-Champaign, in 1989 and 1991, respectively.

Prior to joining the Georgia Institute of Technology, Atlanta, in 1995, he held faculty positions with the University of Illinois at Urbana-Champaign and the University of Hawaii. At the Georgia Institute

of Technology, he holds the Joseph M. Pettit Professorship of Electronics and is currently the Chair for the Electronic Design and Applications Technical Interest Group and the Director of the Georgia Electronic Design Center. With the Georgia Institute of Technology, he heads a research group of 25 members with a focus on integration of high-frequency electronics with optoelectronics and integration of mixed technologies for next-generation wireless and optoelectronic systems. He has authored or coauthored over 200 papers and several book chapters (including three textbooks in development). He has more than 20 patents pending. His research has focused on high-frequency integrated-circuit (IC) design and their integration. His research has produced numerous patents and transfer of technology to industry. Most recently, his research has resulted in the formation of two companies. In 1998, he cofounded the advanced WLAN integrated-circuit company RF Solutions, which is now part of Anadigics. In 2001, he cofounded the next-generation interconnect company Quellan Inc., Atlanta, GA, which develops collaborative signal-processing solutions for enterprise applications, video, storage, and wireless markets.

Dr. Laskar has presented numerous invited talks. For the 2004–2006 term, he has been appointed an IEEE Distinguished Microwave Lecturer for his Recent Advances in High Performance Communication Modules and Circuits seminar. He was a recipient of the 1995 Army Research Office's Young Investigator Award, 1996 recipient of the National Science Foundation (NSF) CAREER Award, 1997 NSF Packaging Research Center Faculty of the Year, 1998 NSF Packaging Research Center Educator of the Year, 1999 corecipient of the IEEE Rappaport Award (Best IEEE Electron Devices Society journal paper), the faculty advisor for the 2000 IEEE Microwave Theory and Techniques Society (IEEE MTT-S) International Microwave Symposium (IMS) Best Student Paper Award, 2001 Georgia Institute of Technology Faculty Graduate Student Mentor of the Year, a 2002 IBM Faculty Award, 2003 Clemson University College of Engineering Outstanding Young Alumni Award, and 2003 Outstanding Young Engineer of the IEEE MTT-S.



**Manos M. Tentzeris** (SM'03) received the Diploma degree in electrical and computer engineering from the National Technical University of Athens, Athens, Greece, in 1992, and the M.S. and Ph.D. degrees in electrical engineering and computer science from The University of Michigan at Ann Arbor, in 1993 and 1998, respectively.

He is currently an Associate Professor with the School of Electrical and Computer Engineering, Georgia Institute of Technology, Atlanta. He has authored or coauthored over 170 papers in refereed

journals and conference proceedings, eight book chapters, and is currently authoring two books. He has helped develop academic programs in highly integrated/multilayer packaging for RF and wireless applications, microwave MEMS, SOP-integrated antennas and adaptive numerical electromagnetics

(finite difference time domain (FDTD), multiresolution algorithms) and heads the ATHENA Research Group (15 researchers). He is the Georgia Institute of Technology National Science Foundation (NSF) Packaging Research Center Associate Director for RF Research and the RF Alliance Leader. He is also the leader of the Novel Integration Techniques Subthrust of the Broadband Hardware Access Thrust of the Georgia Electronic Design Center (GEDC) of the State of Georgia. During the summer of 2002, he was a Visiting Professor with the Technical University of Munich, Munich, Germany, where he introduced a course in the area of high-frequency packaging. He has given more than 40 invited talks in the same area to various universities and companies in Europe, Asia, and the U.S.

Dr. Tentzeris is a member of URSI Commission D, an associate member of EuMA, and a member of the Technical Chamber of Greece. He was the 1999 Technical Program co-chair of the 54th ARFTG Conference, Atlanta, GA, and he is the vice-chair of the RF Technical Committee (TC16) of the IEEE Components, Packaging, and Manufacturing Technology (CPMT) Society. He has organized various sessions and workshops on RF/Wireless Packaging and Integration in IEEE ECTC, IMS, and AP-S Symposia, for all of which he is a member of

the Technical Program Committee in the area of components and RF. He was the recipient of the 2003 National Aeronautics and Space Administration (NASA) Godfrey "Art" Anzic Collaborative Distinguished Publication Award for his activities in the area of finite-ground low-loss low-crosstalk CPWs, the 2003 IBC International Educator of the Year Award, the 2003 IEEE CPMT Outstanding Young Engineer Award for his work on 3-D multilayer integrated RF modules, the 2002 International Conference on Microwave and Millimeter-Wave Technology Best Paper Award (Beijing, China) for his work on compact/SOP-integrated RF components for low-cost high-performance wireless front-ends, the 2002 Georgia Tech-ECE Outstanding Junior Faculty Award, the 2001 ACES Conference Best Paper Award, the 2000 NSF CAREER Award for his work on the development of multiresolution time-domain (MRTD) technique that allows for the system-level simulation of RF integrated modules, and the 1997 Best Paper Award of the International Hybrid Microelectronics and Packaging Society for the development of design rules for low-crosstalk finite-ground embedded transmission lines.